Geomechanics and Engineering, *Vol. 32, No. 1 (2023) 69-84*
https://doi.org/10.12989/gae.2023.32.1.069

Nonlinear shear-flexure-interaction RC frame element on Winkler-Pasternak foundation

Suchart Limkatanyu[1], Worathep Sae-Long*[2], Nattapong Damrongwiriyanupap[2], Piti Sukontasukkul[3], Thanongsak Imjai[4], Thanakorn Chompoorat[2] and Chayanon Hansapinyo[5]

[1]*Department of Civil and Environmental Engineering, Faculty of Engineering, Prince of Songkla University, Songkhla 90110, Thailand*
[2]*Civil Engineering Program, School of Engineering, University of Phayao, Phayao 56000, Thailand*
[3]*Construction and Building Materials Research Center, Department of Civil Engineering, King Mongkut's University of Technology North Bangkok, Bangkok 10800, Thailand*
[4]*School of Engineering and Technology, Walailak University, Nakhorn Si Thammarat 80160, Thailand*
[5]*Center of Excellence in Natural Disaster Management, Department of Civil Engineering, Chiang Mai University, Chiang Mai 50200, Thailand*

(*Received January 6, 2022, Revised December 21, 2022, Accepted December 23, 2022*)

Abstract. This paper proposes a novel frame element on Winkler-Pasternak foundation for analysis of a non-ductile reinforced concrete (RC) member resting on foundation. These structural members represent flexural-shear critical members, which are commonly found in existing buildings designed and constructed with the old seismic design standards (inadequately detailed transverse reinforcement). As a result, these structures always experience shear failure or flexure-shear failure under seismic loading. To predict the characteristics of these non-ductile structures, efficient numerical models are required. Therefore, the novel frame element on Winkler-Pasternak foundation with inclusion of the shear-flexure interaction effect is developed in this study. The proposed model is derived within the framework of a displacement-based formulation and fiber section model under Timoshenko beam theory. Uniaxial nonlinear material constitutive models are employed to represent the characteristics of non-ductile RC frame and the underlying foundation. The shear-flexure interaction effect is expressed within the shear constitutive model based on the UCSD shear-strength model as demonstrated in this paper. From several features of the presented model, the proposed model is simple but able to capture several salient characteristics of the non-ductile RC frame resting on foundation, such as failure behavior, soil-structure interaction, and shear-flexure interaction. This confirms through two numerical simulations.

Keywords: flexure-shear critical members; shear-flexure interaction; soil-structure interaction; Timoshenko frame element; Winkler-Pasternak foundation

1. Introduction

Nowadays, reinforced concrete (RC) is widely employed in construction due to its superior features, such as low cost but high performance, high corrosion resistance, and long service life (Damrongwiriyanupap *et al.* 2015, Tan *et al.* 2016, Prachasaree *et al.* 2018, Mauludin and Oucif 2019, Phoo-Ngernkham *et al.* 2019, Chindaprasirt *et al.* 2022). As a result, this leads to the behavior studies of the RC structures in several applications, such as slab with CFRP strengthening in plates (Chaimahawan and Shaingchin 2019), beam-column joint (Chaimahawan and Pimanmas 2009, Jung *et al.* 2018), precast concrete wall (Chaimahawan *et al.* 2018), column with FRP strengthening (Prachasaree *et al.* 2015, Janwaen *et al.* 2020), etc. The problem of soil-structure interaction is one of those applications and has been of interest in the structural and geotechnical engineering fields for several decades (Limkatanyu *et al.* 2013a, Limkatanyu *et al.* 2014, Sanches *et al.* 2019, Bao and Liu 2020, Qian *et al.* 2021, Limkatanyu *et al.* 2022). Due to the complicated characteristics of soil/foundation, this problem has been studied extensively in both theory and experiments (Whitman and Luscher 1962, Onu 1996, Wankhade and Ghugal 2016, Liu *et al.* 2021). However, to represent the effects of soil-structure interactions on responses of structures for design or investigation of those structures, performance-based numerical models are required. Therefore, this motivates the development of the RC frame model on foundation in this study.

In general, the available numerical models to represent the characteristics of soil-structure interactions within the framework of structural models are divided into two groups, namely: (a) continuous models (Boussinesq 1885, Teodoru 2009); and (b) subgrade models (Limkatanyu *et al.* 2012, Limkatanyu *et al.* 2013a, Limkatanyu *et al.* 2014). Dutta and Roy (2002) and Menglin *et al.* (2011) concluded regarding the merits and disadvantages of these approaches that although the continuous models (Boussinesq 1885, Teodoru 2009) can represent comprehensive responses to varied forces and deformations in the foundation support, the solution of the partial differential equations in this model approach is still a mathematical problem, and a lack

*Corresponding author, Ph.D.
E-mail: worathep.sa@up.ac.th

Copyright © 2023 Techno-Press, Ltd.

ISSN: 2005-307X (Print), 2092-6219 (Online)

of analytical solutions persists. On the other hand, the subgrade models (Limkatanyu *et al.* 2012, Limkatanyu *et al.* 2013a, Limkatanyu *et al.* 2014) are simplified models applied within the structural models. The characteristics of the soil/foundation are modeled with discrete springs attaching along the span of the structure. Therefore, this approach is attractive and can excellently compromise between complexity and simplicity (Ayoub 2003, Limkatanyu *et al.* 2015).

Among the several subgrade models, the Winkler foundation model (Winkler 1867) is the most commonly used in structural engineering community (Limkatanyu *et al.* 2012, Limkatanyu *et al.* 2013b, Limkatanyu *et al.* 2014, Younesian *et al.* 2019) due to its simplicity. The Winkler model (Winkler 1867) assumes that the behaviors of soil/foundation are simulated with non-interconnected transverse springs, while each spring is replaced by the substrate modulus. As a result, this model is often referred to as a "*one-parameter*" foundation model (Zhaohua and Cook 1983). Furthermore, this leads unrealistic responses (discontinuous responses) due to lack of interaction between the Winkler-springs (Limkatanyu *et al.* 2012, Limkatanyu *et al.* 2013b, Younesian *et al.* 2019). To overcome the limitations of the Winkler model, a series of so-called "*two-parameter*" foundation models (Filonenko-Borodich 1940, Pasternak 1954, Hetényi 1971) have been proposed. The concept of the two-parameter foundation model is to have interactions between the Winkler-springs, presented through different medium connectors, such as the tensioned and massless membrane of Filonenko-Borodich (1940), the shear layer of Pasternak (1954), thin plate of Hetényi (1971), etc. In the last two decades, the Pasternak foundation model has been extensively employed to study both static and dynamic responses of structure systems on foundation (Gulkan and Alemdar 1999, Limkatanyu *et al.* 2015, Bao and Liu 2020, Gan *et al.* 2020, Tonzani and Elishakoff 2020, Sae-Long *et al.* 2021a, Karimi *et al.* 2022). For example, Limkatanyu *et al.* (2015) presented the nonlinear displacement-based beam model on Winkler-Pasternak foundation based on the analytical solutions of Gulkan and Alemdar (1999) for the static responses of beam on foundation. Later, Sae-Long *et al.* (2021a) enriched the performance of the beam model on Winkler-Pasternak foundation as proposed by Limkatanyu *et al.* (2015) by formulating the element based on the framework of flexibility-based formulation. Bao and Liu (2020) investigated both the Winkler model and Pasternak model to predict the predominant natural frequency (PNF) for structures partially embedded in soil when compared to experiments based on the work of Prendergast *et al.* (2013). Gan *et al.* (2020) and Tonzani and Elishakoff (2020) used the Pasternak foundation to study the flexure behaviors of a thin plate on foundation and the free vibration frequencies of a beam on foundation, respectively. Karimi *et al.* (2022) investigated the nonlinear vibration and resonance behaviors of a rectangular hyperelastic membrane embedded within the foundation based on the concept of the Winkler-Pasternak model. All mentioned works confirmed the superiority of Pasternak foundation in representing the structure on foundation when compared to the Winkler foundation model (Winkler 1867).

Regarding analysis of a non-ductile RC structure (insufficient details of the transverse reinforcements), it is well-known that the non-ductile RC frame with a low span-to-depth ratio will experience flexure-shear failure (Biskinis *et al.* 2004) or shear failure (Basha and Kaushik 2019). These types of failure are complicated, especially the flexure-shear failure when the inelastic flexural deformation influences the shear resisting force capacity as found in several experiments (Ghee *et al.* 1989, Priestley *et al.* 1993, Li 1994, Lynn 2001, Sezen 2002, Sezen and Moehle 2004). This phenomenon leads to the degradation of the shear force and shear stiffness (Sae-Long and Limkatanyu 2018, Sae-Long *et al.* 2019, Sae-Long *et al.* 2020, Limkatanyu *et al.* 2022), resulting in so-called "*shear-flexure interaction effect*". Therefore, the analysis of non-ductile RC structures needs to consider this effect within the analytical model for the prediction of flexure-shear failure in the structure. In the previous two decades, there were several approaches to consider the interaction effects between shear and flexure within the fiber models, as excellently discussed by Ceresa *et al*. (2007). For example, Marini and Spacone (2006) proposed the fiber frame element for the analysis of the RC frame structures. The interaction between shear and flexure in their model was presented through the shear constitutive relation based on Eurocode 2 (Eurocode 1991) and on enforcing the sectional equilibrium equation within the framework of the force-based formulation. Feng and Xu (2018a) developed the Timoshenko beam-column element with the inclusion of flexure-shear interactions through the multi-dimensional concrete damage model (Feng *et al.* 2018b) while Lodhi and Sezen (2012) introduced the shear-flexure interactions within shear constitutive relation based on the modified compression field theory (MCFT) of Vecchio and Collins (1986). López *et al.* (2022) developed the efficient shear-flexure interaction based on the Multiple-Vertical-Line-Element-Model (MVLEM) of Orakcal *et al.* (2004). The shear-flexure interaction phenomenon of their model was represented by substituting the MVLEM's number of uniaxial elements with the two-dimensional RC panel elements under the membrane actions. Although all the fiber-models mentioned can capture the influences of the interactions between shear and flexure, they lead to complicated material models, high computational costs, and hard computational procedures for the structure models. To address the complications, Sae-Long *et al.* (2019, 2020) presented an alternative shear model considering the shear-flexure interaction effects. Their shear model was modified from the shear force – shear strain relation of Mergos and Kappos (2008, 2012) and was established based on the so-called "*UCSD*" shear-strength model (University of California, San Diego) proposed by Priestley *et al.* (1993). Their model is simple but accurate, which was confirmed in several research works (Sae-Long *et al.* 2019, Sae-Long *et al.* 2020, Sae-Long *et al.* 2021b, Limkatanyu *et al.* 2022). Therefore, this paper employs the shear model of Sae-Long *et al.* (2019, 2020) to represent the shear behaviors of the RC frame and the influence of the shear-flexure interaction effects on the responses in the proposed model.

To the best knowledge of the authors, the RC frame

model on foundation with inclusion of the shear-flexure interaction effects has been only proposed by Sae-Long *et al.* (2021b). However, the frame model on foundation of Sae-Long *et al.* (2021b) is derived based on Winkler-based foundation model. Their model (Sae-Long *et al.* 2021b) does not cover the two-parameter foundation. This limitation motivates developing the fiber RC frame model on foundation in this study. The proposed model extends the fiber RC frame model on Winkler foundation with the shear-flexure interaction effects as proposed by Sae-Long *et al.* (2021b) to cover all the interactions between discrete Winkler-springs through the shear-layer (Pasternak foundation model). Therefore, this is the first proposal of a fiber RC frame model on Winkler-Pasternak foundation with the inclusion of shear-flexure interaction effects. The proposed model is established on the displacement-based finite elements under the kinematic hypothesis of Timoshenko beam theory. Uniaxial material models are employed to represent the nonlinear natures of the RC frame and the foundation.

The content of this study can be summarized as follows. In the first section, the interaction between foundation and structure is introduced through the Winkler-Pasternak foundation model (Pasternak 1954, Limkatanyu *et al.* 2015, Sae-Long *et al.* 2021a). Next, the governing differential equations of the proposed model are presented. This includes equilibrium equations, compatibility equations, and constitutive relations. Then, the displacement-based finite element formulation is proposed through the virtual displacement principle to derive the element stiffness. Subsequently, the shear constitutive relation is next described. In this section, the content includes the UCSD shear-strength model (Priestley *et al.* 1993), the shear force – shear strain relation (Sae-Long *et al.* 2019, Sae-Long *et al.* 2020), and the shear-flexure interaction procedure (Sae-Long *et al.* 2019). Finally, two types of numerical simulations are employed to verify the capability, efficiency, and accuracy of the proposed model. Both simulations are implemented on the general-purpose finite element platform FEAP (Taylor 2000). The first simulation set investigates the convergence of the proposed element, while the second simulation set indicates the importance of the shear-flexure interaction effects to analysis of the non-ductile RC member on foundation, and demonstrates the effects of the shear-layer on the shear responses of the RC frame on foundation when compared to the RC frame model on Winkler foundation.

2. Foundation-structure interaction: Winkler-Pasternak foundation model

The concept of the Winkler-Pasternak foundation model is employed to represent the interactions between foundation and RC frame in this study. The Winkler-Pasternak foundation model is one of the two-parameter foundations (Zhaohua and Cook 1983), originally presented by Pasternak (1954). Under the hypothesis of this foundation model, the characteristic of the foundation is represented by discrete Winkler springs attached with a shear layer. As a result, the drawback of the continuity in the Winkler springs is recovered (Limkatanyu *et al.* 2015). Following that hypothesis, the force-displacement relation for the homogenous and isotropic material is

$$D(x) = k_1 v(x) + k_2 \frac{\partial^2 v(x)}{\partial x^2} \tag{1}$$

where $D(x)$ is the interactive foundation force; k_1 is the stiffness of Winkler springs; k_2 is the Pasternak shear-layer stiffness; and $v(x)$ is the transverse displacement of the frame element.

3. Governing differential equations

3.1 Equilibrium equations

The basic system of the RC frame on foundation under the transverse load $p_y(x)$ in Fig. 1(a) is used in this work. By considering the free body diagram of an infinitesimal segment dx of the basic system, there are two parts in the internal equilibrium equations, such as the RC frame and the shear-layer. Under the small deformation hypothesis, the axial, bending, and transverse equilibrium equations of the RC frame part in Fig. 1(b) are given as follows

$$\frac{dN_{TF}(x)}{dx} = 0 \tag{2}$$

$$\frac{dM_{TF}(x)}{dx} + V_{TF}(x) = 0 \tag{3}$$

$$\frac{dV_{TF}(x)}{dx} + p_y(x) - D_2(x) = 0 \tag{4}$$

where $N_{TF}(x)$ denotes the frame sectional axial force; $V_{TF}(x)$ denotes the frame sectional shear force; $M_{TF}(x)$ denotes the frame sectional bending moment; $p_y(x)$ represents the transverse distributed load; and $D_2(x)$ represents the foundation interactive force.

Considering the infinitesimal segment dx of the shear-layer part in Fig. 1(c), the transverse equilibrium of the shear layer can be presented as

$$\frac{dV_s(x)}{dx} - D_1(x) + D_2(x) = 0 \tag{5}$$

where $V_s(x)$ denotes the sectional shear force of the shear layer; and $D_1(x)$ is the interactive force of the Winkler springs at the bottom of the shear layer as shown in Fig. 1(c).

Substituting Eq. (5) into Eq. (4), the transverse equilibrium equation in Eq. (4) can be rewritten as

$$\frac{dV_{TF}(x)}{dx} + p_y(x) - D_1(x) + \frac{dV_s(x)}{dx} = 0 \tag{6}$$

The equilibrium Eqs. (2), (3), and (6) represent the system equilibrium of the non-ductile RC frame element on Winkler-Pasternak foundation. From these equations, it is noteworthy that there are five internal force unknows, while only three

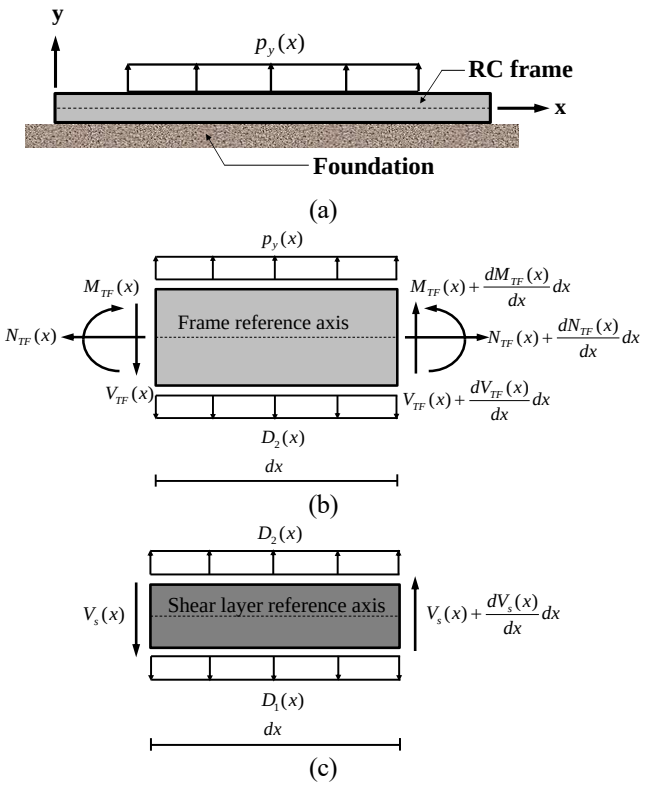

Fig. 1 (a) RC frame on foundation, (b) infinitesimal segment dx of a RC frame element and (c) infinitesimal segment dx of a shear layer

equilibrium equations are available. As a result, this system can be described as an internally statically indeterminate system.

For the sake of simplification, these equations can be grouped into matrix form as

$$\mathbf{L}_T^T\mathbf{D}_T(x)+\mathbf{L}_F^T\mathbf{D}_F(x)-\mathbf{p}(x)=\mathbf{0} \tag{7}$$

in which

$$\begin{aligned}\mathbf{D}_T(x)&=\left\{N_{TF}(x)\quad M_{TF}(x)\quad V_{TF}(x)\right\}^T\\ \mathbf{D}_F(x)&=\left\{D_1(x)\quad V_s(x)\right\}^T\\ \mathbf{p}(x)&=\left\{0\quad 0\quad p_y(x)\right\}^T\end{aligned} \tag{8}$$

where $\mathbf{D}_T(x)$ denotes the frame sectional force vector; $\mathbf{D}_F(x)$ denotes the foundation sectional force vector; $\mathbf{p}(x)$ denotes the external load vector; and $\mathbf{L}_T$ and $\mathbf{L}_F$ are the differential operators defined by

$$\mathbf{L}_T=\begin{bmatrix}\frac{d}{dx} & 0 & 0\\ 0 & \frac{d}{dx} & 0\\ 0 & 1 & -\frac{d}{dx}\end{bmatrix}\quad\text{and}\quad\mathbf{L}_F=\begin{bmatrix}0 & 0 & 1\\ 0 & 0 & -\frac{d}{dx}\end{bmatrix} \tag{9}$$

3.2 Compatibility equations

The sectional deformations can be presented in terms of the sectional displacement through the compatibility relations. For the sake of simplification, the sectional displacements are contained in the displacement vector $\mathbf{u}(x)$ defined as

$$\mathbf{u}(x)=\left\{u(x)\quad\theta(x)\quad v(x)\right\}^T \tag{10}$$

where $u(x)$ and $v(x)$ denote the component displacements in x and y-axis directions; and $\theta(x)$ is the sectional rotation.

In the RC frame part, the frame sectional deformation vector $\mathbf{d}_T(x)$ is the conjugate work pair of the frame sectional force vector $\mathbf{D}_T(x)$ and contains the frame sectional deformations when defined as

$$\mathbf{d}_T(x)=\left\{\varepsilon_{TF}(x)\quad\kappa_{TF}(x)\quad\gamma_{TF}(x)\right\}^T \tag{11}$$

where $\varepsilon_{TF}(x)$ denotes the frame sectional axial strain; $\kappa_{TF}(x)$ denotes the frame sectional bending curvature; and $\gamma_{TF}(x)$ denotes the frame sectional shear strain.

Based on the kinematic assumption of the Timoshenko beam theory (Timoshenko and Gere 1961), the compatibility relations between the frame sectional deformations and the sectional displacements can be expressed as follows (Onate 2013)

$$\varepsilon_{TF}(x)=\frac{du(x)}{dx} \tag{12}$$

$$\kappa_{TF}(x)=\frac{d\theta(x)}{dx} \tag{13}$$

$$\gamma_{TF}(x)=\theta(x)-\frac{dv(x)}{dx} \tag{14}$$

From the compatibility relations in Eqs. (12)-(14), the frame sectional deformation vector $\mathbf{d}_T(x)$ can be written in terms of the displacement vector $\mathbf{u}(x)$ through the differential operator $\mathbf{L}_T$ as

$$\mathbf{d}_T(x)=\mathbf{L}_T\mathbf{u}(x) \tag{15}$$

Similarly, the conjugate work pair of the foundation force vector $\mathbf{D}_F(x)$ is the foundation deformation vector $\mathbf{d}_F(x)$, which can be expressed as

$$\mathbf{d}_F(x)=\left\{\Delta_s(x)\quad\gamma_s(x)\right\}^T \tag{16}$$

where $\Delta_s(x)$ denotes the sectional foundation displacement; and $\gamma_s(x)$ denotes the sectional shear-layer deformation.

Based on the Winkler-Pasternak foundation model (Limkatanyu *et al.* 2015), the compatibility relations between the foundation deformations and the displacement fields can be expressed as

$$\Delta_s(x)=v(x) \tag{17}$$

$$\gamma_s(x)=-\frac{dv(x)}{dx} \tag{18}$$

From the compatibility relations in Eqs. (17) and (18),

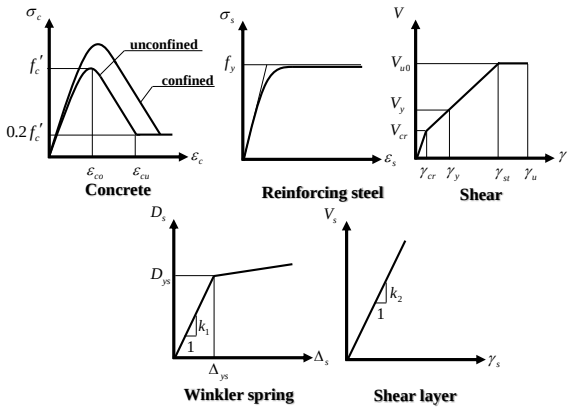

Fig. 2 Force-deformation relations of each material model (Sae-Long *et al.* 2021b)

the foundation sectional deformation vector $\mathbf{d}_F(x)$ can be written in term of the displacement vector $\mathbf{u}(x)$ through the differential operator $\mathbf{L}_F$ as

$$\mathbf{d}_F(x) = \mathbf{L}_F \mathbf{u}(x) \tag{19}$$

It is interesting to point out that there is a contragradient nature between the equilibrium and the compatibility. This can be observed from the equilibrium Eq. (7) and the compatibility Eqs. (15) and (19) in that these equations are related through the differential operators $\mathbf{L}_T$ and $\mathbf{L}_F$.

3.3 Constitutive relations

To describe the nonlinear nature of the force-deformation relations, this study uses uniaxial constitutive laws to represent the characteristics of each used material in the problem of RC frame resting on foundation. It includes the concrete model of Kent and Park (1971), the steel model of Menegotto and Pinto (1973), the shear model of Sae-Long *et al.* (2019, 2020), and the Winkler-Pasternak foundation model of Limkatanyu *et al.* (2015). The force-deformation relations for each material model are illustrated in Fig. 2.

where σ_c and ε_c are, respectively, the concrete stress and strain; f_c' is the concrete strength; ε_{c0} and ε_{cu} are, respectively, the peak and ultimate concrete strain; f_y represents the yield stress of the reinforcing steel bar; V_{cr}, V_y, and V_{u0} are, respectively, the shear force corresponding to the concrete cracking, the first-plastic hinge formation, and its ultimate value; $\gamma_{cr}, \gamma_y, \gamma_{st}$, and γ_u are, respectively, the shear strain associated to the concrete cracking, the first-plastic hinge formation, the transverse reinforcement yielding, and its ultimate value; and D_{ys} and Δ_{ys} denote the foundation yielding force and displacement, respectively.

In the formulation, the nonlinear relations between force and deformation of the RC frame and foundation can be simplified into vector form as follows

$$\mathbf{D}_T(x) = \boldsymbol{\Psi}\left[\mathbf{d}_T(x)\right] \quad \text{and} \quad \mathbf{D}_F(x) = \boldsymbol{\Xi}\left[\mathbf{d}_F(x)\right] \tag{20}$$

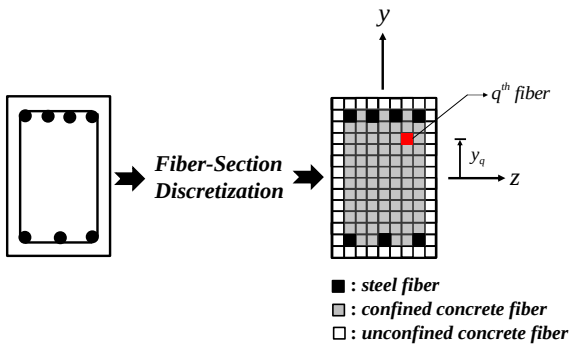

Fig. 3 Fiber-section model (Spacone and Limkatanyu 2000)

The force-deformation relations in Eq. (20) can be written in an incremental form by linearization as

$$\begin{aligned} \mathbf{D}_T(x) &= \mathbf{D}_T^0(x) + \mathbf{k}_T^0(x)\Delta\mathbf{d}_T(x) \\ \mathbf{D}_F(x) &= \mathbf{D}_F^0(x) + \mathbf{k}_F^0(x)\Delta\mathbf{d}_F(x) \end{aligned} \tag{21}$$

where $\mathbf{D}_T^0(x)$ and $\mathbf{k}_T^0(x)$ are, respectively, the initial frame sectional force vector and stiffness matrix; $\mathbf{D}_F^0(x)$ and $\mathbf{k}_F^0(x)$ are, respectively, the initial foundation sectional force vector and stiffness matrix; and superscript 0 on a symbol denotes the initial point of a vector or a matrix for iterative steps.

Based on the fiber-section model (Spacone and Limkatanyu 2000), the element cross-section is refined through the clustering of the cross-section into discrete fibers (layers) as shown in Fig. 3. Following this approach together with the Timoshenko beam theory, the axial and flexural actions automatically interact. Therefore, the sectional axial force and bending moment of the RC frame are obtained by summation of the normal stress and the geometric properties at each fiber. It can be written as

$$N_{TF}(x) = \sum_{q=1}^{nfib} \sigma_q A_q \quad \text{and} \quad M_{TF}(x) = -\sum_{q=1}^{nfib} y_q \sigma_q A_q \tag{22}$$

where y_p, A_p, and σ_p are, respectively, the distance from the reference axis x, the area, and the normal stress of the q^{th} fiber in the section; q denotes a generic fiber; and *nfib* is the amount of fibers in the section.

From the discretization of the sectional forces in Eq. (22), the frame sectional force vector $\mathbf{D}_T(x)$ in Eq. (8) can be rewritten as

$$\mathbf{D}_T(x) = \left\{ \sum_{q=1}^{nfib} \sigma_q A_q \quad -\sum_{q=1}^{nfib} y_q \sigma_q A_q \quad V_{TF}(x) \right\}^T \tag{23}$$

It is important to note that the sectional axial force and bending moment contained in the sectional force vector $\mathbf{D}_T(x)$ depend on the normal stress distribution along the depth of the cross-section based on the fiber-section model (Spacone and Limkatanyu 2000). Conversely, the sectional shear mechanism does not depend on the variation of the force

along the depth of the cross-section. In the other words, the sectional shear mechanism can be represented by only one-fiber discretization.

The sectional stiffness vectors of the RC frame $\mathbf{k}_T(x)$ and foundation $\mathbf{k}_F(x)$ can be expressed based on the fiber-section model (Spacone and Limkatanyu 2000) and the Winkler-Pasternak foundation model (Limkatanyu *et al.* 2015) as

$$\mathbf{k}_T(x)=\begin{bmatrix} \sum_{q=1}^{nfib} E_q A_q & -\sum_{q=1}^{nfib} y_q E_q A_q & 0 \\ -\sum_{q=1}^{nfib} y_q E_q A_q & \sum_{q=1}^{nfib} y_q{}^2 E_q A_q & 0 \\ 0 & 0 & GA_s(x) \end{bmatrix}; \quad \mathbf{k}_F(x)=\begin{bmatrix} k_1(x) & 0 \\ 0 & k_2(x) \end{bmatrix} \tag{24}$$

where $GA_s(x)$ denotes the sectional shear stiffness; and E_q denotes the modulus of the q^{th} fiber in the cross-section. It can be observed from Eq. (24) that the axial and flexural mechanisms do not relate to the shear mechanism directly. However, the shear and flexure interact through the UCSD shear-strength model (Priestley *et al.* 1993) within the shear constitutive model, which will be discussed in section 5.

The equilibrium Eq. (7), the compatibility relations (15) and (19), and the force-deformation Eq. (20) are the core of the governing differential equations for the RC frame problem on Winkler-Pasternak foundation.

4. The displacement-based finite element formulation (Integral state)

4.1 Formulation

In the displacement-based finite element formulation, the element nodal displacements $\mathbf{U}$ are selected as the primary variables, which are employed to approximate the sectional displacement $\mathbf{u}(x)$ through the displacement shape functions $\mathbf{N}_T(x)$. Next, the frame sectional deformations $\mathbf{d}_T(x)$ and the foundation sectional deformation $\mathbf{d}_F(x)$ can be evaluated from the sectional displacements $\mathbf{u}(x)$ based on the compatibility relations in Eqs. (15) and (19). On enforcing the compatibility relations, Eqs. (15) and (19) are satisfied point-by-point along the length of the proposed element. Conversely, the equilibrium Eq. (7) is satisfied in the integral form through the virtual displacement principle.

The equilibrium Eq. (7) can be written in the weighted residual form as follows

$$\int_L \delta\mathbf{u}^T(x)\left[\mathbf{L}_T^T\mathbf{D}_T(x)+\mathbf{L}_F^T\mathbf{D}_F(x)-\mathbf{p}(x)\right]dx=0 \tag{25}$$

where $\delta\mathbf{u}(x)$ is a statically admissible virtual section displacement vector.

Substituting the force-deformation relations of Eq. (21) into Eq. (25) and then enforcing the compatibility relations (15) and (19), Eq. (25) becomes

$$\int_L \delta\mathbf{u}^T(x)\begin{bmatrix}\mathbf{L}_T^T\left(\mathbf{D}_T^0(x)+\mathbf{k}_T^0(x)\mathbf{L}_T\Delta\mathbf{u}(x)\right)+\\ \mathbf{L}_F^T\left(\mathbf{D}_F^0(x)+\mathbf{k}_F^0(x)\mathbf{L}_F\Delta\mathbf{u}(x)\right)-\mathbf{p}(x)\end{bmatrix}dx=0 \tag{26}$$

Applying integration by parts to move the order of the differential equations from the sectional force vectors $\mathbf{D}_T(x)$ and $\mathbf{D}_F(x)$ into the virtual sectional displacement $\delta\mathbf{u}(x)$, Eq. (26) becomes

$$\begin{aligned}&\int_L\left(\mathbf{L}_T\delta\mathbf{u}(x)\right)^T\mathbf{k}_T^0(x)\left(\mathbf{L}_T\Delta\mathbf{u}(x)\right)dx\\ &+\int_L\left(\mathbf{L}_F\delta\mathbf{u}(x)\right)^T\mathbf{k}_F^0(x)\left(\mathbf{L}_F\Delta\mathbf{u}(x)\right)dx\\ &=\delta\mathbf{U}^T\mathbf{P}+\int_L\delta\mathbf{u}^T(x)\mathbf{p}(x)dx\\ &-\int_L\left(\mathbf{L}_T\delta\mathbf{u}(x)\right)^T\mathbf{D}_T^0(x)dx\\ &-\int_L\left(\mathbf{L}_F\delta\mathbf{u}(x)\right)^T\mathbf{D}_F^0(x)dx\end{aligned} \tag{27}$$

where $\delta\mathbf{U}^T\mathbf{P}$ is the external virtual work done by the applied nodal forces $\mathbf{P}$ on the virtual nodal displacements $\mathbf{U}$. This value is obtained from the integration by parts.

To evaluate the displacement fields $\mathbf{u}(x)$ in the displacement-based finite element formulation, the displacement shape function matrix $\mathbf{N}_T(x)$ is employed to predict the displacement fields $\mathbf{u}(x)$ based on the element nodal displacements $\mathbf{U}$ as in

$$\mathbf{u}(x)=\mathbf{N}_T(x)\mathbf{U} \tag{28}$$

Substituting the displacement fields $\mathbf{u}(x)$ of Eq. (28) into Eq. (27) and considering the arbitrariness of $\delta\mathbf{U}$, Eq. (27) becomes

$$\begin{aligned}&\left[\begin{matrix}\int_L\mathbf{B}_T(x)^T\mathbf{k}_T^0(x)\mathbf{B}_T(x)dx\\ +\int_L\mathbf{N}_F(x)^T\mathbf{k}_F^0(x)\mathbf{N}_F(x)dx\end{matrix}\right]\Delta\mathbf{U}\\ &=\mathbf{P}+\int_L\mathbf{N}_T(x)^T\mathbf{p}(x)dx-\int_L\mathbf{B}_T(x)^T\mathbf{D}_T^0(x)dx\\ &-\int_L\mathbf{N}_F(x)^T\mathbf{D}_F^0(x)dx\end{aligned} \tag{29}$$

where $\mathbf{B}_T(x)$ and $\mathbf{N}_F(x)$ are, respectively, the deformation-displacement matrices associated with the RC frame and with the underlying foundation.

The element stiffness equation can be derived from Eq. (29) as

$$\left(\mathbf{K}_T^0+\mathbf{K}_F^0\right)\Delta\mathbf{U}=\left(\mathbf{P}+\mathbf{P}_P\right)-\mathbf{P}_T^0-\mathbf{P}_F^0 \tag{30}$$

where $\mathbf{K}_T^0=\int_L\mathbf{B}_T(x)^T\mathbf{k}_T^0(x)\mathbf{B}_T(x)dx$ is the RC frame element stiffness matrix; $\mathbf{K}_F^0=\int_L\mathbf{N}_F(x)^T\mathbf{k}_F^0(x)\mathbf{N}_F(x)dx$ is the foundation element stiffness matrix; $\mathbf{P}_T^0=\int_L\mathbf{B}_T(x)^T\mathbf{D}_T^0(x)dx$ and $\mathbf{P}_F^0=\int_L\mathbf{N}_F(x)^T\mathbf{D}_F^0(x)dx$ are, respectively, the RC frame and foundation element resisting

force vectors; and $\mathbf{P}_P = \int_L \mathbf{N}_T(x)^T \mathbf{p}(x)dx$ is the equivalent load vector due to the external load vector $\mathbf{p}(x)$.

It is noteworthy that the element stiffness equation (30) represents the core of the stiffness method (displacement-based formulation) for the proposed RC frame element on Winkler-Pasternak foundation as illustrated in Fig. 4. The term on the right-hand-side in Eq. (30) shows the residual force vector corresponding to the integral state of the element equilibrium. This value will vanish when the equilibrium configuration is reached during an incremental iterative solution procedure.

The selection of the displacement shape functions $\mathbf{N}_T(x)$ in Eq. (28) should be done with care due to the so-called "*shear locking phenomenon*" (Mukherjee and Prathap 2001, Beirao da Veiga *et al.* 2012, Senjanovic *et al.* 2013, Sae-Long *et al.* 2019). This problematic event leads to unrealistic predictions of the displacement responses in case of a slender frame, as suggested by Onate (2013). To overcome this problem, this work employs the so-called "*linked displacement shape functions*" suggested by Sae-Long *et al.* (2019) to assess the displacement fields $\mathbf{u}(x)$. The linked displacement shape functions are derived based on the assumption that the sectional transverse displacement $v(x)$ must be of one higher degree than the sectional rotation field $\theta(x)$. As a result, the sectional transverse displacement $v(x)$ can be presented in terms of both the nodal transverse displacements (U_2 and U_5) and the nodal rotations (U_3 and U_6) by enforcing the condition of slender beams ($\gamma_{TF} = 0$). More details to derive the linked displacement shape functions are given in the research work of Sae-Long *et al.* (2019).

The linked displacement shape functions can be written as

$$u(x) = \left(1 - \frac{x}{L}\right)U_1 + \frac{x}{L}U_4 \tag{31}$$

$$\theta(x) = \left(1 - \frac{x}{L}\right)U_3 + \frac{x}{L}U_6 \tag{32}$$

$$v(x) = \left(1 - \frac{x}{L}\right)U_2 + \frac{x}{L}U_5 + \left(\frac{x}{2} - \frac{x^2}{2L}\right)U_3 + \left(-\frac{x}{2} + \frac{x^2}{2L}\right)U_6 \tag{33}$$

where U_1, U_2, U_3, U_4, U_5, and U_6 are the element nodal displacements corresponding to the element nodal forces P_1, P_2, P_3, P_4, P_5, and P_6. The six element nodal displacements are grouped into the element nodal displacement vector $\mathbf{U}$. Based on Eqs. (31)-(33), Sae-Long *et al.* (2019) introduced the displacement shape functions $\mathbf{N}_T(x)$ as follows

$$\mathbf{N}_T(x) = \begin{bmatrix} 1-\frac{x}{L} & 0 & 0 & \frac{x}{L} & 0 & 0 \\ 0 & 0 & 1-\frac{x}{L} & 0 & 0 & \frac{x}{L} \\ 0 & 1-\frac{x}{L} & \frac{x}{2}-\frac{x^2}{2L} & 0 & \frac{x}{L} & -\frac{x}{2}+\frac{x^2}{2L} \end{bmatrix} \tag{34}$$

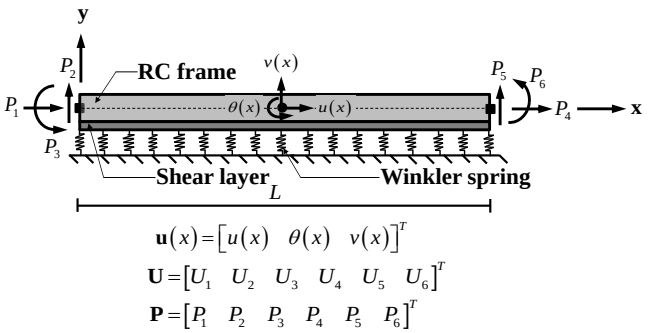

Fig. 4 Proposed frame element on Winkler-Pasternak foundation

The deformation-displacement matrices $\mathbf{B}_T(x)$ and $\mathbf{N}_F(x)$ in Eq. (29) can be defined from the displacement shape functions $\mathbf{N}_T(x)$ in Eq. (34) as

$$\mathbf{B}_T(x) = \mathbf{L}_T\mathbf{N}_T(x) = \begin{bmatrix} -\frac{1}{L} & 0 & 0 & \frac{1}{L} & 0 & 0 \\ 0 & 0 & -\frac{1}{L} & 0 & 0 & \frac{1}{L} \\ 0 & \frac{1}{L} & \frac{1}{2} & 0 & -\frac{1}{L} & \frac{1}{2} \end{bmatrix}; \tag{35}$$

$$\mathbf{N}_F(x) = \mathbf{L}_F\mathbf{N}_T(x) = \begin{bmatrix} 0 & 1-\frac{x}{L} & \frac{x}{2}-\frac{x^2}{2L} & 0 & \frac{x}{L} & -\frac{x}{2}+\frac{x^2}{2L} \\ 0 & \frac{1}{L} & -\frac{1}{2}+\frac{x}{L} & 0 & -\frac{1}{L} & \frac{1}{2}-\frac{x}{L} \end{bmatrix}$$

5. Shear constitutive relation

5.1 UCSD shear-strength model

In order to incorporate the influence of the inelastic flexural mechanism within the shear strength model, a suitable model is required. Among several shear-strength models (Priestley *et al.* 1993, Li 1994, Lynn 2001, Sezen 2002, Sezen and Moehle 2004), the shear model proposed by Priestley *et al.* (1993) is very attractive due to its capability to detect the influence of ductility in the structure. This model was established at the University of California, San Diego and is always called "*UCSD Shear-Strength Model*". Because of its attractive feature, this study employs the UCSD shear-strength model to develop the shear constitutive relation for the analysis of non-ductile RC frame on foundation with inclusion of the shear-flexure interaction effects. The UCSD shear strength V_u as proposed Priestley *et al.* (1993) is composed of three resisting contributions shown in Eq. (36), namely the concrete mechanism, the truss mechanism, and the arch mechanism.

$$V_u = k_\varphi \sqrt{f_c'}\left(0.8A_g\right) + \frac{A_v f_{yv} D'}{s}\cot 30^0 + N\tan\beta \tag{36}$$

where k_φ is a parameter associated with the influence of sectional curvature ductility μ_φ on the shear strength as illustrated in Fig. 5; A_g is gross cross sectional area; f_{yv}, s, and

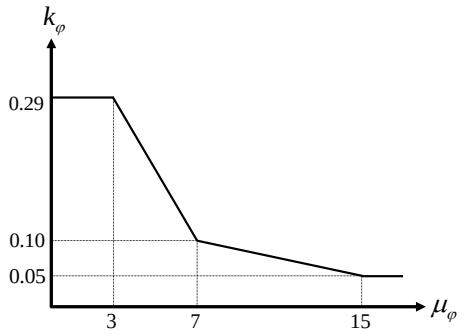

Fig. 5 Factor k_φ and curvature ductility μ_φ relation (Mergos and Kappos 2008)

A_v are, respectively, the yield strength, spacing, and area of transverse reinforcement; N is the compressive load; β is the angle between the column axis and the line connecting the centers of the flexural compression zones at the top and the bottom of the column ends; and D' is the distance measured parallel to the applied shear between centers of the longitudinal reinforcement. It needs to be pointed out that the resisting contribution of arch mechanism in Eq. (36) does not decrease with ductility (Priestley *et al.* 1993).

5.2 Shear force – shear strain relation

In this study, the shear force – shear strain relation starts from the undamaged primary curve as shown in Fig. 6(a). Then, this curve is perturbed to the damaged envelope curve in Fig. 6(b) when the shear-flexure interaction effect is activated. The undamaged primary curve in Fig. 6(a) was originally proposed by Mergos and Kappos (2012) and later modified by Sae-Long *et al.* (2019, 2020). This diagram represents the four behavioral intervals of the non-ductile RC structures, namely before concrete crack (along path O-A), after concrete crack (along path A-B), after flexural yielding (along path B-C), after transverse reinforcement yielding (along path C-D), and shear failure (at point D). Each part in the diagram was described by Sae-Long *et al.* (2019, 2020) and they can be briefly summarized as follows.

The first path O-A presents the elastic behaviors of the RC frame structure. This path connects the origin O to the onset of concrete cracking at point A, with the undamaged shear stiffness $(GA)_0$. The values of the shear force V_{cr} and shear strain γ_{cr} corresponding to the onset of concrete cracking at point A are given by Sezen and Moehle (2004) and can be expressed as follows

$$V_{cr} = \left(\frac{f_t^{'}}{(L_a / h)} \sqrt{\left(1 + \frac{N}{f_t^{'} A_g} \right)} \right) 0.80 A_g \quad \text{and} \quad \gamma_{cr} = \frac{V_{cr}}{(GA)_0} \qquad (37)$$

where $(GA)_0 = 0.80\ GA_g$ denotes the undamaged shear stiffness; G denotes the shear modulus of concrete; L_a / h denotes the shear span ratio; and $f_t^{'}$ denotes the nominal tensile strength of concrete.

The second path A-B represents the characteristic of the concrete post-cracking. This path connects the concrete

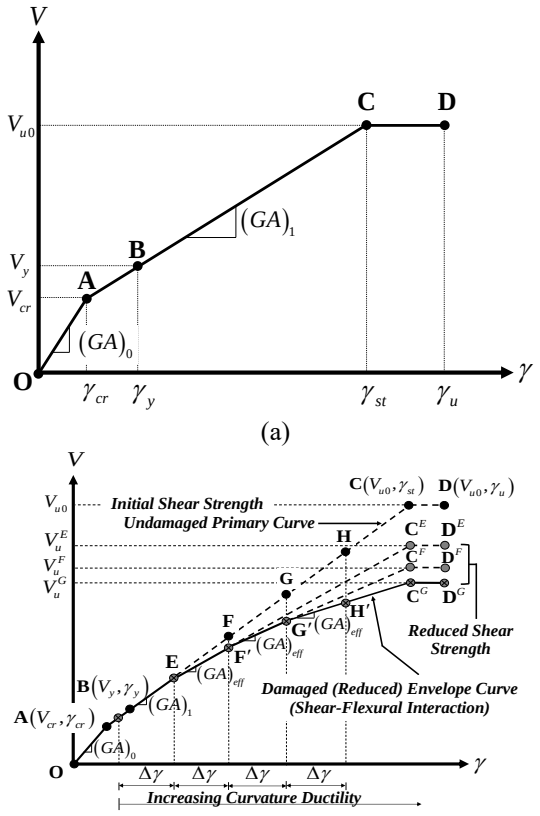

Fig. 6 (a) Undamaged primary curve and (b) Damaged envelope curve (Sae-Long *et al.* 2019)

cracking at point A to the flexural yielding point B at which the plastic hinge forms for the first time within the RC frame member. These points are connected with the shear stiffness $(GA)_1$. The values of shear force V_y and shear strain γ_y corresponding to the onset of the flexural yielding at point B, at which the axial strain in longitudinal reinforcement becomes larger than its yield strain for the first time, are defined through the fiber-section model (Spacone and Limkatanyu 2000).

The third path B-C illustrates the behavior of the RC member after the inelastic flexural deformation. This path connects the flexural yielding at point B and the onset of transverse reinforcement yielding at point C, at which the shear strain reaches shear strain for onset of transverse reinforcement yielding γ_{st}, with the shear stiffness $(GA)_1$.

The final path C-D presents the pre-shear-failure behavior of the non-ductile RC members. The transverse reinforcement yielding at point C links to the shear failure at point D, at which the shear strain reaches the onset of shear failure γ_u.

It can be observed from the primary curve in Fig. 6(a) that the shear strain at the onset of the transverse reinforcement yielding γ_{st} in the third path and the shear strain reaches shear strain at the onset of shear failure γ_u in the final path correspond to the shear strength at ultimate value V_{u0} as defined by the UCSD shear-strength model in Eq. (36). In the

initial state, the initial value of V_u is set to the ultimate shear strength V_{u0}. Then, this value is reduced by the influence of the inelastic flexural deformation, resulting in the variation of shear strength V_u. This leads to the transformation from the undamaged primary curve in Fig. 6(a) into the damaged envelope curve in Fig. 6(b). The values of shear strain γ_{st} and γ_u were suggested by Mergos and Kappos (2012) as follows

$$\gamma_{st} = \kappa \lambda \gamma_{truss} \tag{38}$$

$$\gamma_u = \lambda_1 \lambda_2 \lambda_3 \gamma_{st} \geq \gamma_{st} \tag{39}$$

where κ, λ, λ_1, λ_2, and λ_3 are the modified factors (Mergos and Kappos 2012); γ_{truss} denotes the shear strain at the onset of the transverse reinforcement yielding as derived based on the truss analogy approach (Park and Paulay 1975). These modified factors and the shear strain γ_{truss} can be expressed as

$$\kappa = 1 - 1.07\left(\frac{N}{f_c' A_g}\right); \quad \lambda = 5.37 - 1.59\min\left(2.5, \frac{L_a}{h}\right) \quad \text{for the shear strain } \gamma_{st} \tag{40}$$

$$\lambda_1 = 1 - 2.5\min\left(0.4, \frac{N}{f_c' A_g}\right); \quad \lambda_2 = \min\left(6.25, \frac{L_a^2}{h^2}\right); \quad \lambda_3 = 0.31 + 17.8\min\left(\frac{A_v f_{yv}}{b s f_c'}, 0.08\right) \quad \text{for the shear strain } \gamma_u \tag{41}$$

$$\gamma_{truss} = \frac{V_{cr}}{(GA)_0} + \frac{A_v f_{yv}}{s E_s b \rho_w \sin^4\omega \cot\omega}\left(\sin^4\omega + \frac{E_s}{E_c}\rho_w\right) \tag{42}$$

where ρ_w denotes the volumetric ratio of transverse reinforcement; E_s and E_c are, respectively, the elastic modulus of steel and of concrete; b is the width of cross section; and ω is the angle between frame reference axis and the line of diagonal struts. The optimal angle ω in this study follows the research work of Mergos and Kappos (2012) as about 45°. This value is accepted based on experimental and analytical results.

It needs to be noted that the shear strain γ_{st} and γ_u as introduced by Mergos and Kappos (2012) in Eqs. (38) and (39) were obtained from the modified equation to compromise between experiments and theory through regression analysis.

5.3 Shear-flexure interaction

From the previous subsection 5.2, the reduced shear strength V_u caused by the influence of the inelastic flexural deformation makes the shear stiffness in the path B-C in Fig. 6(b) change. This incident leads to the degradation of both the shear strength and shear stiffness and is named "*shear-flexure interaction*" effect. This interaction effect has been recognized by several researches (Ghee *et al.* 1989, Priestley *et al.* 1993, Li 1994, Lynn 2001, Sezen 2002, Biskinis *et al.* 2004, Sezen and Moehle 2004), pointing out the influence of inelastic flexural deformation on the shear capacity. To take this effect into account in the proposed model, this study follows the procedure of modified shear-flexure interaction of Sae-Long *et al.* (2019, 2020) to capture the degradation of both shear strength and shear stiffness. This procedure was enhanced and modified from the procedure of the shear-flexure interaction proposed by Mergos and Kappos (2012) and was confirmed for capability, efficiency, and accuracy among shear-flexure critical columns and shear critical column (Sae-Long *et al.* 2019).

Based on the displacement-based finite element formulation, the shear force increment ΔV and the sectional shear stiffness $(GA)_{eff}$ are the unknowns and can be evaluated from the shear strain increment $\Delta\gamma$. To approximate both these values, Sae-Long *et al.* (2019) established the so-called "*reference*" shear stiffness referring to the undamaged state and the analytical state. The reference shear stiffness $\left(GA_{ref}\right)_i^k$ is

$$\left(GA_{ref}\right)_i^k = \frac{\left(V_0\right)_i^{k+1} - V^k}{\Delta\gamma_i^k} \tag{43}$$

where $\left(V_0\right)_i^{k+1} = V_{cr} + \left(GA\right)_1\left(\gamma_i^{k+1} - \gamma_{cr}\right)$ denotes the non-reduced shear strength corresponding to the shear strain $\gamma_i^{k+1} = \gamma^k + \Delta\gamma_i^k$; and i and k are, respectively, the element iterative step and the load increment.

Considering the geometric relation of shear force to shear strain, it can be defined as

$$\Delta\gamma_i^k = \frac{\Delta V_i^k}{\left(GA_{eff}\right)_i^k} = \frac{\Delta V_i^k + \left(\Delta V_c^{\deg}\right)_i^k}{\left(GA_{ref}\right)_i^k} \tag{44}$$

where $\left(\Delta V_c^{\deg}\right)_i^k$ denotes the degradation of the shear strength due to increase in flexural deformation. This parameter can be determined from the following equation

$$\left(\Delta V_c^{\deg}\right)_i^k = \left(GA_{ref}\right)_i^k \Delta\gamma_i^k - \left(\frac{\left(V_u\right)_i^k - V^k}{\gamma_{st} - \gamma^k}\right)\Delta\gamma_i^k \tag{45}$$

The shear stiffness $\left(GA_{eff}\right)_i^k$ is obtained from Eq. (44) by solving in terms of the reference shear stiffness $\left(GA_{ref}\right)_i^k$ as follows:

$$\left(GA_{eff}\right)_i^k = \frac{\Delta V_i^k}{\Delta V_i^k + \left(\Delta V_c^{\deg}\right)_i^k}\left(GA_{ref}\right)_i^k \tag{46}$$

It needs to be noted that the shear stiffness $\left(GA_{eff}\right)_i^k$ and the increment of the shear force ΔV_i^k in Eq. (46) are unknown and mutually dependent. To evaluate both, a subscript index

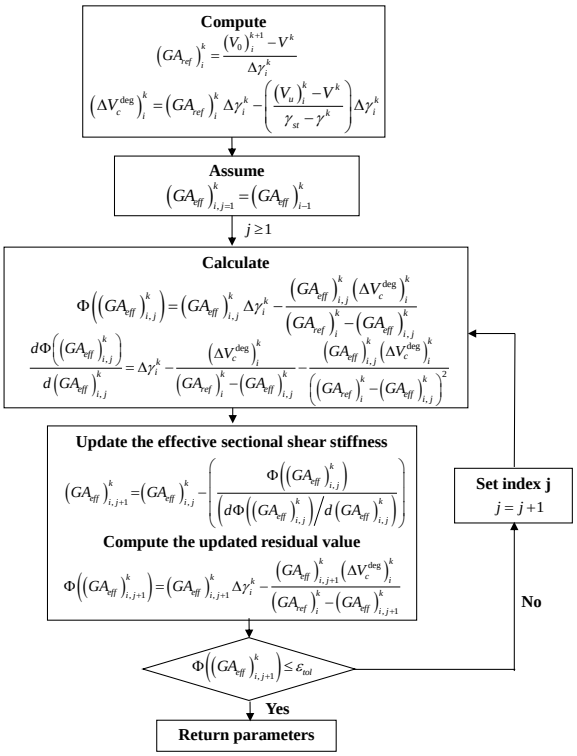

Fig. 7 Flow chart of iterative shear-flexure interaction procedure (Sae-Long *et al.* 2019)

"j" is given to both parameters $\left(GA_{eff}\right)_i^k$ and ΔV_i^k as counter of iterative steps within the procedure for shear-flexure interactions. Both values are obtained by requiring that the residual function $\Phi\left(\left(GA_{eff}\right)_{i,j}^k\right)$ is less than a specific tolerance ε_{tol}. This function is established by numerical solution with the Newton-Raphson method (Chapra and Canale 2002). The residual function $\Phi\left(\left(GA_{eff}\right)_{i,j}^k\right)$ and its derivative can be expressed as

$$\Phi\left(\left(GA_{eff}\right)_{i,j}^k\right) = \left(GA_{eff}\right)_{i,j}^k \Delta\gamma_i^k - \frac{\left(GA_{eff}\right)_{i,j}^k \left(\Delta V_c^{\deg}\right)_i^k}{\left(GA_{ref}\right)_i^k - \left(GA_{eff}\right)_{i,j}^k} \quad (47)$$

$$\frac{d\Phi\left(\left(GA_{eff}\right)_{i,j}^k\right)}{d\left(GA_{eff}\right)_{i,j}^k} = \Delta\gamma_i^k - \frac{\left(\Delta V_c^{\deg}\right)_i^k}{\left(GA_{ref}\right)_i^k - \left(GA_{eff}\right)_{i,j}^k} - \frac{\left(GA_{eff}\right)_{i,j}^k \left(\Delta V_c^{\deg}\right)_i^k}{\left(\left(GA_{ref}\right)_i^k - \left(GA_{eff}\right)_{i,j}^k\right)^2} \quad (48)$$

The procedures to evaluate the shear stiffness $\left(GA_{eff}\right)_i^k$ and the increment of the shear force ΔV_i^k are summarized in Fig. 7. This procedure is called "*modified shear-flexure interaction process*" and is discussed in more detail in the works of Sae-Long *et al.* (2019, 2020).

6. Numerical simulations

In this paper, two numerical simulations are employed to assess the capability, efficiency, and accuracy of the proposed RC frame element on the Winkler-Pasternak foundation model for the analysis of non-ductile RC frame resting on foundation. The first simulations are convergence studies, which simulate both global and local responses of the proposed model. The second simulation assesses the importance of considering shear-flexural interactions in an analysis of the non-ductile RC frame on foundation and the effects of the shear layer on the shear responses. Both simulations use the so-called "*flexure-shear critical columns*" (Biskinis *et al.* 2004), which failed in shear following flexural yielding, to present the behaviors of the non-ductile RC frame. Furthermore, the columns in both simulations were verified for accuracy of the shear model of Sae-Long *et al.* (2019, 2020) by matching experimental and analytical results. Therefore, both columns can be employed to represent the behaviors of the non-ductile RC frame resting on foundation.

6.1 Simulation I: Convergence studies

The first simulation presents convergence study of the responses of the proposed frame model on Winkler-Pasternak foundation at both the global and local levels. A simply supported RC frame on the foundation system shown in Fig. 8 is employed to investigate the convergence behaviors and to confirm the accuracy and efficiency of the proposed model. The frame-foundation system is subjected to a midspan displacement under displacement-control and a constant compressive load at its tips of 667 kN. The properties of the RC frame come from column 2CLD12, which represented a flexural-shear critical column (Mergos and Kappos 2008). The material properties of this column are given by Sezen (2002), such as concrete strength f_c' of 21 MPa, yield stress of longitudinal reinforcement f_{yl} of 434 MPa, and yield stress of transverse reinforcement f_{yv} of 476 MPa. The geometric properties of this column are illustrated in Fig. 8. Furthermore, this study uses the properties of the Winkler-Pasternak foundation model as proposed in the work of Sapountzakis and Kampitsis (2013) to represent the behaviors of the foundation medium. The Winkler spring model is assumed to be elastic-perfectly plastic with an initial stiffness k_1 of 20 MPa and yielding foundation force D_{ys} of 60 kN/m while the shear layer is assumed to be elastic with stiffness k_2 of 5,000 kN. To present all analytical responses in this paper, each proposed element uses the seven Gauss-Lobatto integration points and the discretized frame cross-section with forty fibers (layers). This amount is sufficient to demonstrate the analytical responses for the displacement-based finite element formulation and has been proven in several research works (Sae-Long *et al.* 2019, Sae-Long *et al.* 2021b). From Fig. 8, the frame-foundation system can be reduced to only a half by use of symmetry.

Fig. 9(a) demonstrates the convergence study of the midspan force – midspan deflection at the global level.

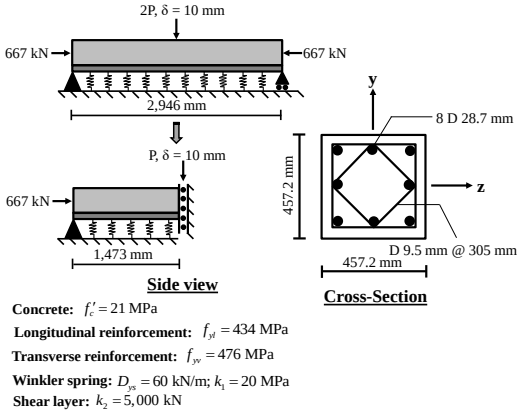

Fig. 8 Simulation I: Convergence studies

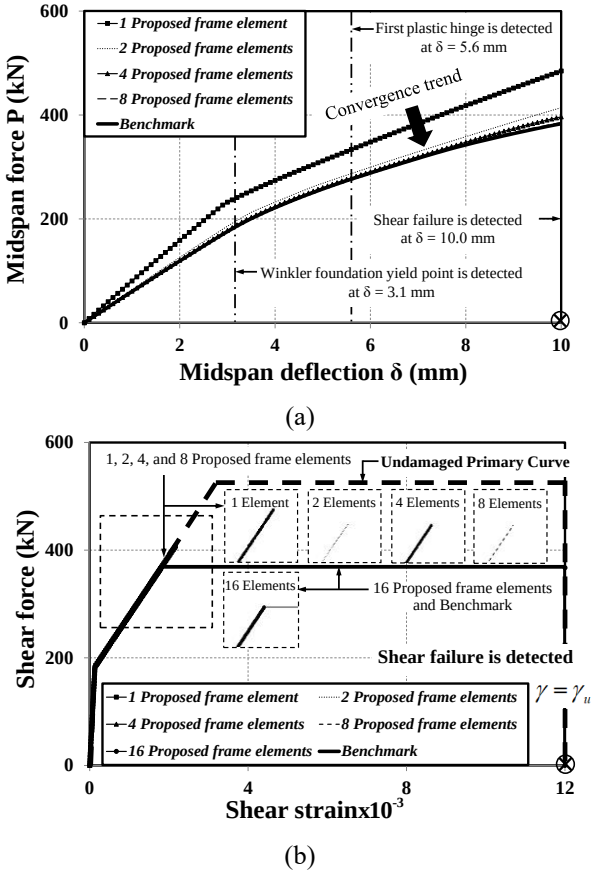

Fig. 9 (a) Global response and (b) Local response

Different meshes of the proposed elements are employed in this diagram. From this diagnostic diagram, a "*benchmark*" result is obtained from the response of 16 of the proposed elements, while 8 proposed elements are enough to match the benchmark response. Furthermore, this diagram shows that there are three occurrences in this simulation, namely the Winkler-spring yielding at the midspan deflection of 3.1 mm, the first plastic hinge formation in the RC frame at the midspan deflection of 5.6 mm, and the detection of shear failure at the midspan deflection of 10.0 mm.

Fig. 9(b) illustrates the shear force – shear strain relation at the midspan with a deflection of 10.0 mm. This diagram shows that the local responses (shear force – shear strain relation) require a more refined mesh than the global responses in Fig. 9(a). Thus, the benchmark case at the local level is doubled from 16 to 32 proposed elements, while only 16 proposed elements are enough to converge to the benchmark response. In these responses, the first plastic-hinge formation is found at the shear strain of about $\gamma_y = 9.2x10^{-4}$ and is detected at only the location with the midspan deflection due to the restrain and load conditions. The shear envelope curve starts to deviate from the undamaged primary curve to the damaged envelope curve when the value of the current sectional curvature exceeds 3. This characteristic occurs due to the shear-flexural interaction effect as governed by the UCSD shear-strength model (Priestley *et al.* 1993) within the shear constitutive model. It can be observed that the shear strain increases rapidly when the shear-flexural interaction is activated. Finally, the shear failure occurs when the shear strain reaches its ultimate value of about $\gamma_u = 12x10^{-3}$. This value corresponds well with to the experimental observations as predicted by Mergos and Kappos (2012).

It needs to be noted in the diagnostic responses in Fig. 9 that the prediction of the shear failure and the plastic-hinge formation is require sufficiently refined meshes. This is clear in Fig. 9(b) showing that 2, 4, and 8 of the proposed elements can closely present the maximum shear force. However, these elements cannot capture the shear failure due to the lack of accuracy to predict the curvature ductility demand within the plastic hinge region. It doesn't surprise that 16 elements of the proposed model can capture the failure point and the plastic-hinge formation in the state of an inelastic flexure deformation due to a sufficiently refined mesh to predict the sectional curvature ductility demand.

6.2 Simulation II: Effect of shear-flexure interaction and influence of foundation on RC frame responses

The second simulation demonstrates the shear-flexure interactions and soil-structure interaction effects on the responses of non-ductile RC frame on foundation. A simply supported RC frame on Winkler-Pasternak foundation as illustrated in Fig. 10 is the typical system to study in this simulation. The properties of the RC frame imitate the flexure-shear critical column, namely 2CMH18 as reported by Lynn (2001). The geometry and material properties of this column are presented in Fig. 10 and can be expressed as: concrete compressive strength f_c' 25.5 MPa, yield stress of longitudinal reinforcement f_{yl} 331 MPa, and yield stress of transverse reinforcement f_{yv} 400 MPa. The properties of the Winkler-Pasternak foundation follow those used in simulation I, in that the Winkler spring is defined to be elastic-perfectly plastic while the shear layer is assumed to be elastic. To compare the effects of shear-flexure interactions and soil-structure interactions on both global and local frame responses, there are five different diagnostic models, namely: (a) proposed frame-foundation model; (b) classical Timoshenko frame model on Winkler-Pasternak foundation, (c) shear-flexure interaction frame model on Winkler foundation (Sae-Long *et al.* 2021b), (d) classical frame model on Winkler foundation, and (e) the

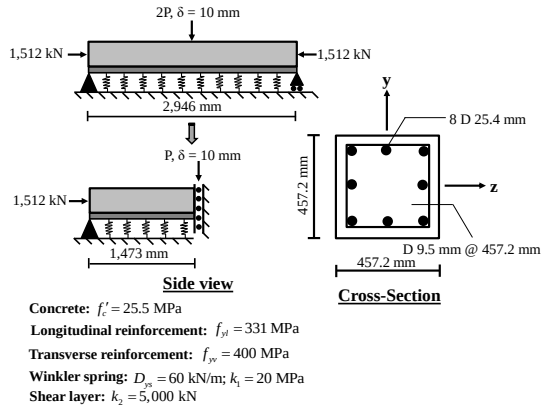

Fig. 10 Simulation II: RC frame on foundation

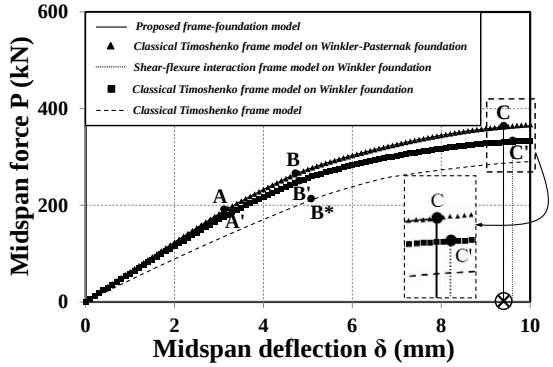

Fig. 11 Global response of simulation II

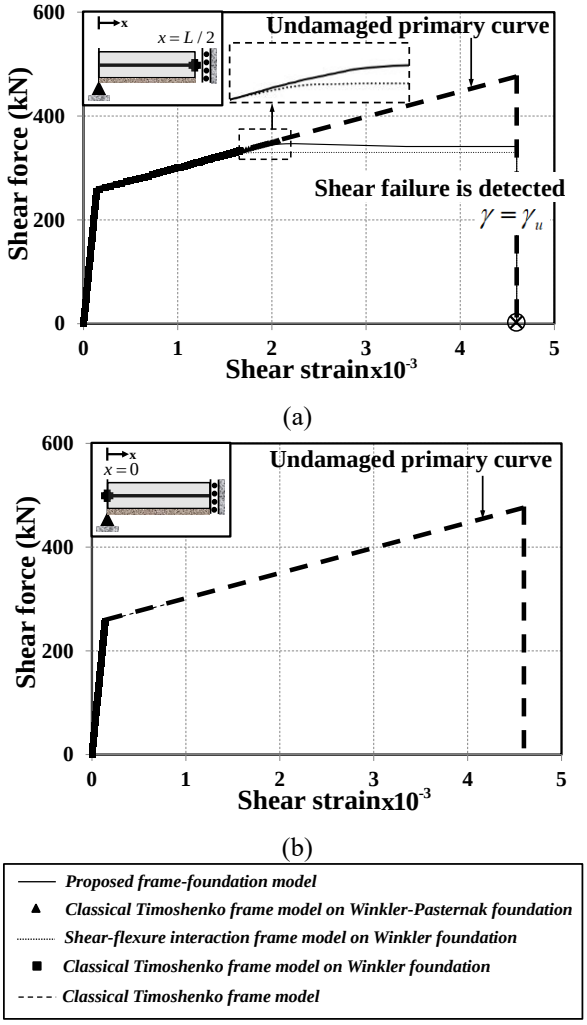

Fig. 12 (a) Local responses inside the plastic hinge region at the midspan (x=L/2) and (b) Local responses outside the plastic hinge region at the support (x=0)

classical Timoshenko frame model. The so-called "*classical*" in the analytical models denotes the numerical model that doesn't consider the effect of the shear-flexure interaction within the models. Furthermore, this study uses 16 elements with 7 Gauss-Lobatto integration points per element and the discretized frame cross-section with forty fibers (layers) for all responses of each analytical model. This amount of elements is sufficient for the prediction of inelastic responses, as proven in simulation I and several research works (Sae-Long *et al.* 2019, Sae-Long *et al.* 2021b).

Fig. 11 presents the global response (force-displacement at the midspan) as analyzed from the five different numerical models. This plot reveals that the soil-structure interaction effect makes the element become stiffer and stronger. This stiffening phenomenon is in good agreement with both experiments and theories in the literature (Zhaohua and Cook 1983, Gulkan and Alemdar 1999, Dutta and Roy 2002, Ayoub 2003, Menglin *et al.* 2011, Limkatanyu *et al.* 2012, Limkatanyu *et al.* 2013, Limkatanyu *et al.* 2014, Limkatanyu *et al.* 2015, Wankhade and Ghugal 2016, Sanches *et al.* 2019, Bao and Liu 2020, Tonzani and Elishakoff 2020, Liu *et al.* 2021, Qian *et al.* 2021, Sae-Long *et al.* 2021a, Limkatanyu *et al.* 2022). The influence of the additional shear layer within the series of the Winkler-Pasternak foundation models is more pronounced than the Winkler-based model and the classical model without the soil-structure interaction. From this diagram, there are three events in this simulation, namely the yielding of the Winkler spring (Point A and A'), the first plastic-hinge formation within the RC frame models (Point B, B', and B*), and the shear failure (Point C and C'). The position of the transverse displacement at point A and A' as obtained from the models on foundation is similar with the midspan deflection δ of 3.1 mm, while the initial stiffness of the frame models on Winkler-Pasternak foundation is larger than the initial stiffness of the frame models on Winkler foundation by about 1.07 fold. Next, the deflection at the plastic-hinge formation within the frame element is clearly influenced by the soil-structure interaction. The frame models on Winkler-Pasternak foundation predict the formation of the first plastic hinge at the deflection δ of 4.7 mm, while these values obtained from the frame models on Winkler foundation and the frame model without foundation are about 4.8 mm and 5.1 mm, respectively. Moreover, the yielding force corresponding to the first plastic-hinge formation is about 1.06 and 1.25 fold that of the frame models on Winkler foundation and the frame model without foundation, respectively. Finally, it is interesting to observe in this diagram that the series of the classical frame model cannot capture the shear failure at point C and C' due to the lack of the inclusion of the shear-

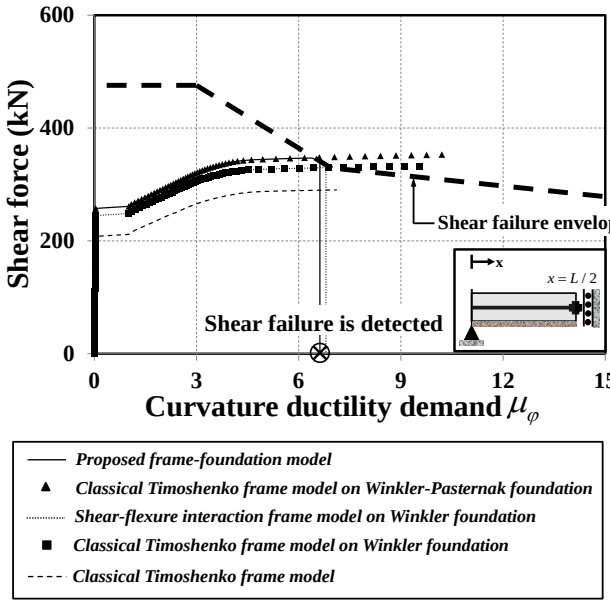

Fig. 13 Shear force versus curvature ductility inside the plastic hinge region (x=L/2)

flexure interaction effect within these models while the proposed model and the Winkler-based frame model considering the shear-flexure interaction effect (Sae-Long *et al.* 2021b) can detect this failure behavior at the midspan deflection δ of 9.5 mm (point C) and 9.6 mm (point C'), respectively. This confirms the superiority of the proposed model when compared to a series of classical models.

Figs. 12(a) and 12(b) present the shear force – shear strain relation (local responses) inside (x=L/2) and outside (x=0) the plastic hinge region, respectively. This diagram is obtained from the five different diagnostic models. From the analysis of the shear response inside the plastic-hinge region as shown in Fig. 12(a), it is interesting to observe that the series of classical models cannot predict the failure behavior of this system, while the proposed model and the frame model with inclusion of shear-flexure interaction effect are able to capture the shear failure. The failure is detected when the shear strain in both models reaches the shear strain at the onset of shear failure $\gamma_u = 4.6x10^{-3}$ based on the shear constitutive model. This value corresponds to the midspan deflections at point C and C' in Fig. 11, respectively. Furthermore, the effect of the shear layer in the Winkler-Pasternak foundation on local response makes shear stiffness increase, similarly as observed in the global response in Fig. 11. On the other hand, in local responses outside the plastic hinge region in Fig 12(b), the shear force – shear strain relations obtained from the five numerical models are almost identical. This is due to the fact that the plastic hinge formation is not activated in this region.

Fig. 13 superimposes the shear force – curvature ductility relations inside the plastic hinge region (x=L/2) obtained from the five numerical frame models. The dashed line in this diagram represents the shear capacity envelope established based on the UCSD shear-strength model (Priestley *et al.* 1993) in Eq. (36). From assessing this diagram, it can be seen that the classical models on foundation lack the consideration of shear-flexure interaction resulting in a fiasco in predicting the shear failure. Although the shear force in these models meets the shear capacity, the failure doesn't occur in these models. Conversely, the proposed model and the shear-flexure-interaction frame model on Winkler foundation (Sae-Long *et al.* 2021b) can detect the shear failure when the shear force reaches the shear capacity. The maximum shear force as predicted by the proposed model is larger than the maximum shear force of the frame model on Winkler foundation (Sae-Long *et al.* 2021b) by about 8.51%, while the curvature ductility is lesser by about 2.7% due to the system-stiffness enhancement from the shear layer. Furthermore, this diagram indicates that the inclusion of shear-flexure interaction effects is important for the analysis of non-ductile RC frame model on foundation. This simulation demonstrated that this frame system would not have failed in shear when the shear-flexure interaction had not been activated.

7. Conclusions

This paper proposes a novel frame element on Winkler-Pasternak foundation with the inclusion of shear-flexure interaction effects for the analysis of non-ductile reinforced concrete (RC) frame on foundation. The proposed element is derived in a displacement-based formulation under the kinematic assumptions of Timoshenko beam theory. The uniaxial material models for concrete, steel bar, shear, and foundation are employed to represent the nonlinear natural characteristics of each material. The shear constitutive model considers the shear-flexure interaction effect, which is defined through the UCSD shear-strength model. This effect is activated when the inelastic flexural deformation influences the shear capacity in the concrete. As a result, the shear resisting force and shear stiffness are reduced. This was confirmed in two sets of numerical simulations. The convergence studies in the first set of simulations confirmed capability, efficiency, and accuracy of the proposed model, while the second simulation showed the necessity of considering shear-flexure interaction effects in the analysis of non-ductile RC frame on foundation. Furthermore, the shear layer within the Winkler-Pasternak model makes the shear responses stiffer and stronger when compared to the Winkler-based frame model, as discussed in diagnosing the second simulation set. Finally, it can be concluded that the proposed model can capture several characteristics of the RC frame on foundation, such as the soil-structure interactions, the degradation of shear capacity due to the shear-flexure interaction effects, and the shear failure characteristics.

In the next steps to develop the new frame model on foundation, the authors will extend the model to cover the three-parameter foundation model and to cover the bond-interface slip effect. Lastly, the authors hope this paper will be applicable to practical engineering works and will be useful for other interested researchers.

Acknowledgments

The financial support of this work was provided by the Office of the Permanent Secretary, Ministry of Higher Education, Science, Research and Innovation (Grant No. RGNS 64-134), by the Thailand Research Fund (Grant No. RTA 6280012) and by the Thailand Science Research and Innovation Fund and the University of Phayao (Grant No. FF66-UoE023). Furthermore, we would like to sincerely thank the copy-editing service of Research and Development Office, and Assoc. Prof. Dr. Seppo Karrila who dedicated his time to provide valuable comments, and gratefully acknowledge the support and assistance received.

References

Ayoub, A. (2003), "Mixed formulation of nonlinear beam on foundation elements", *Comput. Struct.*, **81**(7), 411-421. https://doi.org/10.1016/S0045-7949(03)00015-4.

Bao, T. and Liu, Z.L. (2020), "Evaluation of Winkler model and Pasternak model for dynamic soil-structure interaction analysis of structures partially embedded in soils", *Int. J. Geomech.*, **20**(2), 04019167. https://doi.org/10.1061/(ASCE)GM.1943-5622.0001519.

Basha, S.H. and Kaushik, H.B. (2019), "Investigation on improving the shear behavior of columns in masonry infilled RC frames under lateral loads", *Bull. Earthq. Eng.*, **17**, 3995-4026. https://doi.org/10.1007/s10518-019-00622-3.

Beirao da Veiga, V., Lovadina, C. and Reali, A. (2012), "Avoiding shear locking for the Timoshenko beam problem via isogeometric collocation methods", *Comput. Method. Appl. Mech. Eng.*, **241-244**, 38-51. https://doi.org/10.1016/j.cma.2012.05.020.

Biskinis, D., Roupakias, G. and Fardis, M. (2004), "Degradation of shear strength of reinforced concrete members with inelastic cyclic displacement", *ACI Struct. J.*, **101**(6), 773-783. https://doi.org/10.14359/13452.

Boussinesq, H. (1885), *Applications des Potentiels al'Etude de l'Equilibre et du Mouvement des Solids Elastique*, Gauthier-Villars, Paris, France.

Ceresa, P., Petrini, L. and Pinho, R. (2007), "Flexure-shear fiber beam-column elements for modeling frame structures under seismic loading: State of the art", *J. Earthq. Eng.*, **11**(1), 46-88. https://doi.org/10.1080/13632460701280237.

Chaimahawan, P. and Pimanmas, A. (2009), "Nonlinear FEM analysis of RC beam-column joint strengthened by cast in-situ joint expansion", *J. Adv. Concr. Technol.*, **7**(3), 307-326. https://doi.org/10.3151/jact.7.307.

Chaimahawan, P., Hansapinyo, C. and Phuriwarangkhakul, P. (2018), "Test and finite element analysis of gravity load designed precast concrete wall under reversed cyclic loads", *Eng. J.*, **22**(2), 185-200. https://doi.org/10.4186/ej.2018.22.2.185.

Chaimahawan, P. and Shaingchin, S. (2019), "Deflection control of reinforced concrete slab strengthened with CFRP plates", *J. Eng. Sci. Technol.*, **14**(6), 3387-3405.

Chapra, S.C. and Canale, R.P. (2002), *Numerical methods for engineers*, McGraw-Hill, New York, USA.

Chindaprasirt, P., Lao-un, J., Zaetang, Y., Wongkvanklom, A., Phoo-ngernkham, T., Wongsa, A. and Sata, V. (2022), "Thermal insulating and fire resistance performances of geopolymer mortar containing auto glass waste as fine aggregate", *J. Build. Eng.*, **60**, 105178. https://doi.org/10.1016/j.jobe.2022.105178.

Damrongwiriyanupap, N., Limkatanyu, S. and Xi, Y. (2015), "A thermo-hygro-coupled model for chloride penetration in concrete structures", *Adv. Mater. Sci. Eng.*, 682940. https://doi.org/10.1155/2015/682940.

Dutta, S.C. and Roy, R.A. (2002), "Critical review on idealization and modeling for interaction among soil-foundation-structure system", *Comput. Struct.*, **80**(20-21), 1579-1594. https://doi.org/10.1016/S0045-7949(02)00115-3.

Eurocode No. 2 (1991), *Design of concrete structures-part 1-1: General rules and rules for buildings*, ENV 1992-1-1; Brusse, Belgium.

Feng, D.C. and Xu, J. (2018a), "An efficient fiber beam-column element considering flexure–shear interaction and anchorage bond-slip effect for cyclic analysis of RC structures", *Bull. Earthquake Eng.*, **16**, 5425-5452. https://doi.org/10.1007/s10518-018-0392-y.

Feng, D.C., Ren, X.D. and Li, J. (2018b), "Softened damage-plasticity model for analysis of cracked reinforced concrete structures", *J. Struct. Eng.*, **144**(6), 04018044. https://doi.org/10.1061/(ASCE)ST.1943-541X.0002015.

Filonenko-Borodich, M.M. (1940), "Some approximate theories of the elastic foundation", *Uch. Zap. Mosk. Gos, Univ. Mekh.*, **46**, 3-18.

Gan, J., Yuan, H. and Li, S. (2020), "A computing method for bending problem of thin plate on Pasternak foundation", *Adv. Mech. Eng.*, **12**(7), 168781402093933. https://doi.org/10.1177/1687814020939333.

Ghee, A., Priestley, M.J.N. and Paulay, T. (1989), "Seismic shear strength of circular reinforced concrete columns", *ACI Struct. J.*, **86**(1), 45-59.

Gulkan, P. and Alemdar, B.N. (1999), "An exact finite element for a beam on a two-parameter elastic foundation: A revisit", *Struct. Eng. Mech.*, **7**(3), 259-276. https://doi.org/10.12989/sem.1999.7.3.259.

Hetényi, M. (1971), *Beams on elastic foundation: theory with applications in the fields of civil and mechanical engineering*, University of Michigan, Ann Arbor, Michigan, USA.

Janwaen, W., Barros, J.A.O. and Costa, I.G. (2020), "New hybrid FRP strengthening technique for rectangular RC columns subjected to eccentric compressive loading", *J. Compos. Constr.*, **24**(5), 4020043. https://doi.org/10.1061/(ASCE)CC.1943-5614.0001052.

Jung, W., Kim, J. and Kwon, M. (2018), "Performance evaluation of RC beam-column joints with different bonding interfaces", *Sci. Iran.*, **25**(1), 11-21. https://doi.org/10.24200/sci.2017.4175.

Karimi, S., Ahmadi, H. and Foroutan, K. (2022), "Nonlinear vibration and resonance analysis of a rectangular hyperelastic membrane resting on a Winkler–Pasternak elastic medium under hydrostatic pressure", *J. Vib. Control*, https://doi.org/10.1177/10775463211062339.

Kent, D.C. and Park, R. (1971), "Flexural members with confined concrete", *J. Struct. Div.*, **97**(7), 1964-1990. https://doi.org/10.1061/JSDEAG.0002957.

Li, X. (1994), "Reinforced concrete columns under seismic lateral force and varying axial load", Ph.D. Dissertation, Department of Civil Engineering, University of Canterbury, Christchurch, New Zealand.

Limkatanyu, S., Kuntiyawichai, K., Spacone, E. and Kwon, M. (2012), "Natural stiffness matrix for beams on Winkler foundation: exact force-based derivation", *Struct. Eng. Mech.*, **42**(1), 39-53. https://doi.org/10.12989/sem.2012.42.1.039.

Limkatanyu, S., Prachasaree, W., Damrongwiriyanupap, N., Kwon, M. and Jung, W. (2013a), "Exact stiffness for beams on Kerr-type foundation: the virtual force approach", *J. Compos. Constr.*, 626287. https://doi.org/10.1155/2013/626287.

Limkatanyu, S., Kuntiyawichai, K., Spacone, E. and Kwon, M. (2013b), "Nonlinear Winkler-based beam element with improved displacement shape functions", *KSCE J. Civ. Eng.*,

17, 192-201. https://doi.org/10.1007/s12205-013-1606-0.

Limkatanyu, S., Prachasaree, W., Damrongwiriyanupap, N. and Kwon, M. (2014), "Exact stiffness matrix for nonlocal bars embedded in elastic foundation media: the virtual-force approach", *J. Eng. Math.*, **89**, 163-176. https://doi.org/10.1007/s10665-014-9707-4.

Limkatanyu, S., Sae-Long, W., Prachasaree, W. and Kwon, M. (2015), "Improved nonlinear displacement-based beam element on a two-parameter foundation", *Eur. J. Environ. Civ. Eng.*, **19**(6), 649-671. https://doi.org/10.1080/19648189.2014.965847.

Limkatanyu, S., Sae-Long, W., Damrongwiriyanupap, N., Imjai, T., Chaimahawan, P. and Sukontasukkul, P. (2022), "Shear-flexure interaction frame model on Kerr-type foundation for analysis of non-ductile RC members on foundation", *J. Appl. Comput. Mech.*, **8**(3), 1076-1090. https://doi.org/10.22055/jacm.2022.39597.3440.

Liu, W., Tian, Y. and Cassidy, M.J. (2021), "An interface to numerically model undrained soil-structure interactions", *Comput. Geotech.*, **138**(5), 104327. https://doi.org/10.1016/j.compgeo.2021.104327.

Lodhi, M.S. and Sezen, H. (2012), "Estimation of monotonic behavior of reinforced concrete columns considering shear-flexure-axial load interaction", *Earthquake Eng. Struct. Dyn.*, **41**(15), 2159-2175. https://doi.org/10.1002/eqe.2180.

López, C.N., Massone, L.M. and Kolozvari, K. (2022), "Validation of an efficient shear-flexure interaction model for planar reinforced concrete walls", *Eng. Struct.*, **252**, 113590. https://doi.org/10.1016/j.engstruct.2021.113590.

Lynn, A.C. (2001), "Seismic evaluation of existing reinforced concrete building columns", Ph.D. Dissertation, Department of Civil and Environmental Engineering, University of California, Berkeley, USA.

Marini, A. and Spacone, E. (2006), "Analysis of reinforced concrete elements including shear effects", *ACI Struct. J.*, **103**(5), 645-655. https://doi.org/10.14359/16916.

Mauludin, L.M. and Oucif, C. (2019), "Modeling of self-healing concrete: A review", *J. Appl. Comput. Mech.*, **5**, 526-539. https://doi.org/10.22055/jacm.2017.23665.1167.

Menegotto, M. and Pinto, P.E. (1973), "Method of analysis for cyclically loaded reinforced concrete plane frames including changes in geometry and nonelastic behavior of elements under combined normal force and bending", *Proceedings of the IABSE Symp. Resist. Ultimate Deformability Struct. Acted on by Well-Defined Repeated Loads*, Lisbon.

Menglin, L., Huaifeng, W., Xi, C. and Yongmei, Z. (2011), "Structure-soil-structure interaction: Literature review", *Soil Dyn. Earthquake Eng.*, **31**(12), 1724-1731. https://doi.org/10.1016/j.soildyn.2011.07.008.

Mergos, P.E. and Kappos, A.J. (2008), "A distributed shear and flexural flexibility model with shear-flexure interaction for R/C members subjected to seismic loading", *Earthq. Eng. Struct. D.*, **37**(12), 1349-1370. https://doi.org/10.1002/eqe.812.

Mergos, P.E. and Kappos, A.J. (2012), "A gradual spread inelasticity model for R/C beam-columns, accounting for flexure, shear and anchorage slip", *Eng. Struct.*, **44**, 94-106. https://doi.org/10.1016/j.engstruct.2012.05.035.

Mukherjee, S. and Prathap, G. (2001), "Analysis of shear locking in Timoshenko beam elements using the function space approach", *Commun. Numer. Method. Eng.*, **17**(6), 385-393. https://doi.org/10.1002/cnm.413.

Onate, E. (2013), *Structural analysis with the finite element method volume 2: beams, plates and shells*, Springer, Netherlands.

Onu, G. (1996), "Equivalences in the soil-structure interaction", *Comput. Struct.*, **58**(2), 367-380. https://doi.org/10.1016/0045-7949(95)00129-5.

Orakcal, K., Wallace, J.W. and Conte, J.P. (2004), "Nonlinear modeling and analysis of slender reinforced concrete walls", *ACI Struct. J.*, **101**(5), 688-698.

Park, R. and Paulay, T. (1975), *Reinforced concrete structures*, John Wiley & Sons, New York, USA.

Pasternak, P.L. (1954), *On a new method of analysis of an elastic foundation by means of two constants*, Gosudarstvennoe Izdatelstvo Literaturi po Stroitelstvu I Arkhitekture, Moscow, Russia.

Phoo-Ngernkham, T., Hanjitsuwan, S., Li, L.Y., Damrongwiriyanupap, N. and Chindaprasirt P. (2019), "Adhesion characterisation of Portland cement concrete and alkali-activated binders", *Adv. Cem. Res.*, **31**(2), 69-79. https://doi.org/10.1680/jadcr.17.00122.

Prachasaree, W., Sangkaew, A., Limkatanyu, S. and GangaRao, H.V.S. (2015), "Parametric study on dynamic response of fiber reinforced polymer composite bridges", *Int. J. Polym. Sci.*, Article No 565301. https://doi.org/10.1155/2015/565301.

Prachasaree, W., Limkatanyu, S., Wangapisit, O. and Kraidam, S. (2018), "Field investigation of service performance of concrete bridges exposed to tropical marine environment", *Int. J. Civ. Eng.*, **16**(12), 1757-1769. https://doi.org/10.1007/s40999-017-0250-3.

Prendergast, L.J., Hester, D., Gavin, K. and O'Sullivan, J.J. (2013), "An investigation of the changes in the natural frequency of a pile affected by scour", *J. Sound Vib.*, **332**(25), 6685-6702. https://doi.org/10.1016/j.jsv.2013.08.020.

Priestley, M.J.N., Seible, F., Verma, R. and Xiao, Y. (1993), "Seismic shear strength of reinforced concrete columns", Structural Systems Research Project Report No. SSRP 93/06; University of California, San Diego, USA.

Qian, J., Mu, L., Zhang, Y. and Zhang, Y. (2021), "Behavior of a structured piled beam–slab foundation for a wind turbine under multidirectional loads in sand", *Int. J. Geomech.*, **21**(3), 04020267. https://doi.org/10.1061/(ASCE)GM.1943-5622.0001934.

Sae-Long, W. and Limkatanyu, S. (2018), "Shear model with shear-flexure interaction for non-linear analysis of reinforced concrete frame element", *MATEC Web Conf.*, **192**, 02003. https://doi.org/10.1051/matecconf/201819202003.

Sae-Long, W., Limkatanyu, S., Prachasaree, W., Horpibulsuk, S. and Panedpojaman, P. (2019), "Nonlinear frame element with shear-flexure interaction for seismic analysis of non-ductile reinforced concrete columns", *Int. J. Concr. Struct. Mater.*, **13**, 32. https://doi.org/10.1186/s40069-019-0343-2.

Sae-Long, W., Limkatanyu, S., Hansapinyo, C., Imjai, T. and Kwon, M. (2020), "Forced-based shear-flexure-interaction frame element for nonlinear analysis of non-ductile reinforced concrete columns", *J. Appl. Comput. Mech.*, **6**, 1151-1167. https://doi.org/10.22055/jacm.2020.32731.2065.

Sae-Long, W., Limkatanyu, S., Hansapinyo, C., Prachasaree, W., Rungamornrat, J. and Kwon, M. (2021a), "Nonlinear flexibility-based beam element on Winkler-Pasternak foundation", *Geomech. Eng.*, **24**(4), 371-388. https://doi.org/10.12989/gae.2021.24.4.371.

Sae-Long, W., Limkatanyu, S., Panedpojaman, P., Prachasaree, W., Damrongwiriyanupap, N., Kwon, M. and Hansapinyo, C. (2021b), "Nonlinear Winkler-based frame element with inclusion of shear-flexure interaction effect for analysis of non-ductile RC members on foundation", *J. Appl. Comput. Mech.*, **7**(1), 148-164. https://doi.org/10.22055/jacm.2020.34699.2460.

Sanches, R., Simões, F.M.F. and Pinto da Costa, A. (2019), "Physical and geometrical nonlinear dynamic analysis of beams on foundations under moving loads", *J. Eng. Mech.*, **146**(1), 04019114. https://doi.org/10.1061/(ASCE)EM.1943-7889.0001692.

Sapountzakis, E.J. and Kampitsis, A.E. (2013), "Inelastic analysis of beams on two-parameter tensionless elastoplastic

foundation", *Eng. Struct.*, **48**, 389-401. https://doi.org/10.1016/j.engstruct.2012.09.012.
Senjanovic, I., Vladimir, N. and Cho, D.S. (2013), "A shear locking-free beam finite element based on the modified Timoshenko beam theory", *Trans. FAMENA*, **37**(4), 1-16.
Sezen, H. (2002), "Seismic behavior and modeling of reinforced concrete building columns", Ph.D. Dissertation, Department of Civil and Environmental Engineering, University of California, Berkeley, USA.
Sezen, H. and Moehle, J.P. (2004), "Shear strength model for lightly reinforced concrete columns", *J. Struct. Eng.*, **130**(11), 1692-1703. https://doi.org/10.1061/(ASCE)0733-9445(2004)130:11(1692).
Spacone, E. and Limkatanyu, S. (2000), "Responses of reinforced concrete members including bond-slip effects", *ACI Struct. J.*, **97**(6), 831-839. https://doi.org/10.14359/9628.
Tan, Y.-Z., Liu, Y.-X., Wang, P.-Y. and Zhang, Y. (2016), "A predicting model for thermal conductivity of high permeability-high strength concrete materials", *Geomech. Eng.*, **10**(1), 49-57. https://doi.org/10.12989/gae.2016.10.1.049.
Taylor, R.L. (2000), *FEAP: A finite element analysis program*, User manual: version 7.3, Department of Civil and Environmental Engineering, University of California, Berkeley, USA.
Teodoru, I.B. (2009), "Beams on elastic foundation. the simplified continuum approach", *Bull. Polytech. Inst. Jassy*, **LV**(LIX), 37-46.
Timoshenko, S.P. and Gere, J.M. (1961), *Theory of elastic stability engineering societies monographs*, McGraw-Hill Book Company, New York, USA.
Tonzani, G.M. and Elishakoff, I. (2020), "Three alternative versions of the theory for a Timoshenko–Ehrenfest beam on a Winkler–Pasternak foundation", *Math. Mech. Solids*, **26**(3), 299-324. https://doi.org/10.1177/1081286520947775.
Vecchio, F.J. and Collins, M.P. (1986), "The modified compression-field theory for reinforced concrete elements subjected to shear", *ACI J., Proc.*, **83**(2), 219-231. https://doi.org/10.14359/10416.
Wankhade, R. and Ghugal, Y.M. (2016), "Study on soil-structure interaction: A review", *Int. J. Eng. Res.*, **5**(3), 737-741. https://doi.org/10.17950/ijer/v5i3/047.
Whitman, R.V. and Luscher, U. (1962), "Basic experiment into soil-structure interaction", *ASCE Soil Mech. Found. Div. J.*, **88**(2), 135-167. https://doi.org/10.1061/JSFEAQ.0000461.
Winkler, E. (1867), *Theory of elasticity and strength*, Dominicus, Prague, Czechoslovakia.
Younesian, D., Hosseinkhani, A., Askari, H. and Esmailzadeh, E. (2019), "Elastic and viscoelastic foundations: A review on linear and nonlinear vibration modeling and applications", *Nonlinear Dyn.*, **97**, 853-895. https://doi.org/10.1007/s11071-019-04977-9.
Zhaohua, F. and Cook, R.D. (1983), "Beam elements on two-parameter elastic foundations", *J. Eng. Mech.*, **109**(6), 1390-1402. https://doi.org/10.1061/(ASCE)0733-9399(1983)109:6(1390).